Highly increased capacitance and thermal stability of anodic oxide films on oxygen-incorporated Zr-Ti alloy

H. Habazaki[1,*], K. Kobayashi[1], E. Tsuji[1], C. Zhu[1], Y. Aoki[1], S. Nagata[2]

[1]Division of Applied Chemistry, Faculty of Engineering, Hokkaido University, Sapporo, Hokkaido 060-8628, Japan

[2]Institute for Materials Research, Tohoku University, 2-1-1, katahira, Aoba-ku, Sendai 980-8577, Japan

*Corresponding author: Phone & Fax: +81-11-706-6575, e-mail: habazaki@eng.hokudai.ac.jp

Abstract

Heat treatment of Zr-24 at% Ti alloy with barrier-type dielectric anodic oxide films was conducted at 473 K in air to examine the thermal stability of the dielectric oxide films for possible electrolytic capacitor application. The anodic oxide film was formed by anodizing of the alloy at 50 V for 30 min in 0.1 mol dm^{-3} ammonium pentaborate electrolyte. The anodic oxide film of 125 nm thickness was crystalline, containing both monoclinic and tetragonal ZrO_2 phase. It was found that marked thickening of the oxide film with generation of cracks occurred during heat treatment at 473 K. Thus, the dielectric loss was largely increased along with the capacitance increase. In contrast, the anodic oxide film formed on the oxygen-incorporated alloy remained uniform and no significant increase in dielectric loss was observed even after the heat treatment. The capacitance of the anodic film became as high as 4.8 mF m^{-2}, which was nearly twice that on Ta. The high capacitance was associated with the preferential formation of tetragonal ZrO_2 phase in the anodic oxide film on the oxygen-incorporated alloy. Findings indicated that the oxygen-incorporated Zr-Ti alloy is a promising novel material for capacitor application.

Keywords; anodic oxide, Zr-Ti alloy, dielectric material, anodizing

1. Introduction

Anodizing of metals and alloys is of practical importance for many applications, including surface treatments of aluminum and magnesium practical alloys for corrosion protection, wear resistance and surface decoration [1-3], production of Al and Ta electrolytic capacitors [4-8] and fabrication of nanomaterials for functional devices [9-11]. Both compact, so-called barrier-type anodic films and porous-type anodic films are formed on a range of metals, depending upon anodizing conditions. The most important practical application of the barrier-type anodic films is the use as a dielectric layer in electrolytic capacitors. Ta capacitors consist of porous Ta anode sintered from Ta powder, a thin dielectric layer formed by anodizing of the Ta anode and conducting polymer or MnO_2

cathode.

Ta capacitors possess superior properties, such as high reliability, high volume efficiency and low equivalent series resistance [7]. However, because of limited natural resources of Ta and relatively high cost of Ta raw material, there is a continuous demand of the development of alternative materials for electrolytic capacitor. Niobium is a candidate since its physical and chemical properties are similar to those of Ta and the anodizing behavior of these two metals is also similar to each other. It is, however, often claimed that the reliability of niobium capacitor is lower than that of Ta one, because of higher susceptibility of field crystallization of anodic niobium oxide [12-18], which increases dielectric loss of the capacitor, and large bias potential dependence of the capacitance originating from the n-type semiconductor character of the niobium oxide [19]. Alloying of niobium to form a non-equilibrium, uniform solid solution is effective in suppressing the field crystallization and avoiding the degradation of the dielectric properties [14,15,20-23], although the non-equilibrium solid-solution alloys are not suitable for application to the current capacitor technology, which includes high temperature sintering of the metal powders.

Ti is also an abundant element and forms an anodic oxide with relatively high permittivity, but shows an amorphous-to-crystalline transition at low formation voltages less than 10 V. The transition induces gas generation on the crystalline oxide, making the anodic films highly defective [24-26]. Again, alloying of Ti is effective in suppressing the amorphous-to-crystalline transition, and the amorphous anodic films formed on the solid-solution Ti alloys are promising as dielectric films for capacitor application [27-30]. These anodic oxide films are also promising for a hybrid inorganic-organic field effect transistor [31,32]. However, Ti shows limited solubility to many alloying elements including silicon, tungsten, molybdenum and aluminum at equilibrium. It is not easy to form solid solution Ti alloy anode by sintering of the alloy powders for capacitor application.

A Ti-Zr alloy system is interesting because of the formation of solid solution in a wide composition range at equilibrium. In addition, it was reported that the capacitances of the anodic films formed on the Ti-Zr alloys were markedly enhanced at the Zr-rich alloy composition, where

nanocrystalline ZrO_2 phase precipitated in the amorphous oxide matrix [33]. The capacitance of the anodic films on the Zr-rich Zr-Ti alloy was higher than that on Ta and the band gap of 3.65 for the anodic oxide film formed on Zr-20 at% Ti alloy was larger than that on TiO_2 (3.1-3.2) [34]. Such Zr-Ti alloy may become a promising novel material for the electrolytic capacitor application. For practical application, it is important to investigate the thermal stability of the anodized Zr-Ti alloy, particularly since both Zr and Ti are highly reactive with oxygen and the solubility of oxygen to both metals are relatively high.

In this study, we investigated the change in the thickness, structure and dielectric properties of the anodic films on a Zr-Ti alloy during heat treatment at 473 K in air. We also prepared the anodic film on an oxygen-incorporated Zr-Ti alloy to examine the influence of incorporated oxygen in alloy on the thermal degradation of the anodized alloy. Here, we report marked improvement of the thermal stability and further increase in the capacitance of the anodic film by the oxygen incorporation in alloy.

2. Experimental

The Zr-Ti alloy containing 24 at% Ti was prepared by magnetron sputtering (Shimadzu, SP-2C system) on glass or silicon wafer substrate. The glass substrate of 1 mm thickness was degreased in an aqueous solution containing 30 g dm^{-3} surfactant (Okuno Chemical, Top Alclean 30) at 333 K and the silicon wafer substrate was thermally oxidized at 1173 K in air to form a thermal oxide film. The target consisted of 99.9% Ti disc of 100 mm in diameter and 6 pieces of 99.9% Zr discs of 20 mm in diameter; the latter discs were placed symmetrically on the sputter erosion region of the Ti disc target. After installing the substrates and targets in the sputtering chamber, the chamber was evacuated to less than 5×10^{-5} Pa and then, alloy deposition was conducted under ~0.3 Pa argon at 0.5 A for 30 min. In order to get the deposited alloy films of uniform composition and thickness, the substrate holders were rotated around the central axis of the chamber as well as their own axes. The composition of the alloy film was determined by Rutherford backscattering spectroscopy and the thickness of the deposited film, determined by cross-sectional SEM observation was ~490 nm.

The incorporation of oxygen in the deposited alloy was performed by anodizing and subsequent heat treatment in vacuum. The deposited Zr-Ti alloy was anodized to several formation voltages at a constant current density of 50 A m^{-2} in 0.01 mol dm^{-3} ammonium pentaborate electrolyte at 293 K. Then, the anodized specimen was heat-treated at 823 K for 1 h in vacuum at $<10^{-3}$ Pa. The dielectric oxide films were finally formed by anodizing of the as-deposited and oxygen-incorporated Zr-Ti alloy specimens at a constant current density of 50 A m^{-2} to 50 V with current decay for 30 min in 0.01 mol dm^{-3} ammonium pentaborate electrolyte at 293 K. All anodizing experiments were performed using a two-electrode cell and a platinum sheet was used as a counter electrode. Thermal degradation of the anodized specimens were examined by heating at 473 K in air for various periods of time.

Dielectric properties of the anodic oxide films were examined by an electrochemical impedance spectroscopy (EIS). The measurements were conducted in 0.1 mol dm^{-3} ammonium pentaborate electrolyte by applying 50 mV (rms) sinusoidal alternating voltage at an open circuit potential using a NF Block, 5020 frequency analyzer combined with a Hokuto Denko, HA-500 potentiostat. The obtained spectra were fitted using a Zsimpwin software.

Phases in the specimens were identified by a glazing incidence X-ray diffraction (GI-XRD) method. A Rigaku, RINT-2200 system with Cu Kα radiation (λ = 0.15418 nm) was used and the incident angle, α, was set to 1°. Surfaces of the specimens were observed by a JEOL, JSM-6500F field emission scanning electron microscope operated at 10 kV, while cross-sections of some specimens were observed by a JEOL, JEM-2000FX transmission electron microscope operated at 200 kV. Electron-transparent sections were prepared by a Hitachi, FB-2100 focused ion beam system. Prior to ion beam thinning, the surfaces were coated with platinum to avoid damaging the anodic oxide films.

Depth profile analysis of the anodized specimens was conducted using a Jobin-Yvon, 5000RF glow discharge optical emission spectroscopy (GDOES). The profiles were obtained at 13.56 MHz, 40 W and argon pressure of 900 Pa by monitoring the characteristic wavelengths of 365.350 nm (Ti), 339.198 nm (Zr), 249.678 nm (B), 165.701 (C) and 130.217 nm (O) with a sampling time of 0.1 s

during RF sputtering.

The composition of each layer of the specimens was also examined by Rutherford backscattering spectroscopy (RBS) using a 2 MeV He^{2+} ion beam supplied by a tandem-type accelerator at Tohoku University. The scattered particles were detected at 170° to the incident beam direction, which was normal to the specimen surface. The energy of the backscattered ions was calibrated using a following equation:

$$E\ (\text{keV}) = 75.9 + 4.36 \times (\text{Channel Number}) \quad (1)$$

The data were analyzed using a RUMP program [35].

3. Results and Discussion

Figure 1 shows transmission electron micrographs of the as-deposited alloy specimens anodized at 50 V before and after heat treatment at 473 K in air for 72 h. An anodic oxide film of uniform thickness with flat and parallel alloy/film and film/electrolyte interfaces is developed before heat treatment (Fig. 1a). The thickness of the anodic oxide film is 125 ± 3 nm, corresponding to the formation ratio of 2.50 ± 0.06 nm V^{-1}. This ratio on the Zr-24 at% Ti alloy is slightly smaller than that on Zr (2.70 nm V^{-1}) [36]. The reduction of film thickness by the addition of Ti is consistent with a previous study [33]. The anodic oxide film shown in Fig. 1a shows diffraction contrast, indicating that the film is crystalline. High resolution micrograph of the anodic oxide (Fig. 1c) reveals obviously the presence of lattice fringes. Further, the analysis of the spacing of the lattice fringes and the fast Fourier transformation image shown in Fig. 1c disclose the presence of both monoclinic ZrO_2 (m-ZrO_2) and tetragonal-ZrO_2 (t-ZrO_2) phases. The former phase is thermodynamically stable at room temperature, while the latter is the high-temperature phase. It is well known that doping of metallic ions in ZrO_2 stabilizes the high-temperature form even at ambient temperature. The presence of the two phases in the anodic oxide films is in agreement with the anodic oxide films formed on Zr-20 at% Ti alloy [33].

The relative molar ratio of the two ZrO_2 phases was dependent upon the Ti content, and further increase in the Ti content resulted in an increase in the molar ratio of t-ZrO_2. It is worth mentioning that cubic ZrO_2 (c-ZrO_2), which is also a high-temperature phase of ZrO_2, has similar diffraction pattern to t-ZrO_2. Raman study is useful to distinguish the t-ZrO_2 and c-ZrO_2 and it was reported that the anodic films formed on Zr-Si alloys contained t-ZrO_2, not c-ZrO_2 [37]. Thus, we assumed the formation of t-ZrO_2 phase, not c-ZrO_2, also in the anodic films on the present Zr-Ti alloy. Figure 1b shows the transmission electron micrograph of the cross-section of the anodized specimen after heat treatment at 473 K for 72 h. It is obvious that the thickness of the anodic oxide film increases remarkably from 125 ± 3 nm to 224 ± 3 nm as a consequence of thermal oxidation of the alloy at temperature as low as 473 K.

Elemental depth profiles of the anodized specimens before and after heat treatment for 72 h were measured by GDOES (Fig. 2). Slightly wavy profiles of Zr and Ti in the oxide films shown in Fig. 2 is an artefact, which arises from the interference of light emitted from the respective elements. Figure 2a shows the elemental depth profile of the anodized specimen before heat treatment. Both Ti and Zr in the anodic film distribute throughout the film thickness. Boron species are incorporated in the outer part of the anodic film from electrolyte. This is also consistent with previous studies [28,33]. The incorporated boron species are suitable as a novel marker to understand the diffusing species in thickening the oxide film during heat treatment in air at 473 K. Figure 2b shows the elemental depth profile of the anodized specimen after heat treatment. The increased sputtering time for the oxide film in comparison with the specimen before heat treatment (Fig. 2a) discloses thickening of the oxide film during heat treatment, which is in agreement with the TEM observations shown in Fig. 1. Boron species are located at the surface region of the oxide film even after heat treatment. The peak intensity of boron is higher after heat treatment (Fig. 2b) in comparison with that before heat treatment (Fig. 2a), but the integrated peak areas of boron in the outer part of the oxide films are similar to each other, indicating the similar amount of boron species in both the specimens. The location of the boron species indicates that oxide thickening during heat treatment proceeds mainly due to inward diffusion

of oxide ions, not outward diffusion of cation species. This is consistent with the fact that ZrO_2 is an oxide ion conductor at elevated temperatures. Although high oxide ion conductivity is known for c-ZrO_2, m-ZrO_2 also shows oxide ion diffusion at elevated temperatures [38].

The composition and density of the anodic oxide films before and after heat treatment were further examined quantitatively using RBS. Figure 3 shows experimental and simulated RBS spectra of the anodized specimens before and after heat treatment at 473 K for 72 h. The simulated spectra obtained using thicknesses, compositions and densities shown in Table 1 fitted well with the experimental spectra. In the simulation, the presence of boron was neglected because of low sensitivity. Table 1 shows that the cationic ratio of Ti to Zr in the anodic films before and after heat treatment is similar to the alloy composition, and the ratio is constant throughout the film thickness. The formation of the single layer anodic films is associated with the predominant oxide formation at the alloy/film interface by inward migration of oxide ions during growth of the anodic films consisting mainly of crystalline phases [39,28]. Subsequent thermal oxidation of the anodized specimen also proceeded mainly due to inward diffusion of oxide ions, as discussed above. Thus, simple thickening of the oxide film with the film composition unchanged occurred during heat treatment. However, the density of the anodic oxide films, which was estimated using the film thickness obtained by TEM, increased from 4.14 to 4.50 g cm^{-3} after heat treatment. The increased density may be associated with the improved crystallinity of the anodic oxide film as shown in XRD patterns (Fig. 4). The XRD patterns also indicate the increased relative ratio of t-ZrO_2 phase with respect to m-ZrO_2 after heat treatment.

Since significant thermal oxidation occurred during heat treatment of the anodized Zr-Ti alloy at temperature as low as 473 K, an attempt of oxygen incorporation to the alloy film was made to reduce the thermal oxidation. The oxygen incorporation into alloy was conducted by pre-anodizing of the magnetron-sputtered alloy film and subsequent heat treatment at 823 K in vacuum. Figure 5a shows XRD patterns of the specimens anodized to various voltages, followed by heat treatment at 823 K. After anodizing, crystalline m-ZrO_2 and t-ZrO_2 phases were observed, similar to Fig. 4. However, after heat treatment at 823 K, ZrO_2 phases are absent as shown in Fig. 5a. Only an hcp alloy phase is

identified for the specimens pre-anodized to 25 V and 50 V, while additional peaks identified to a Zr_3O phase are detected for the specimens pre-anodized to 80 V and 150 V. The absence of the ZrO_2 phases after heat treatment suggests the absorption of oxygen species in the anodic oxide films into the alloy film. This was confirmed from the shift of the peak angle for the 103 reflection of the hcp alloy phase. The change in the (103) lattice spacing with the pre-anodizing voltage, plotted in Fig. 5b, shows marked increase in the lattice spacing at the lower pre-anodizing voltage, and almost saturation of the expansion of the lattice spacing at and above 50 V. The lattice expansion of the alloy phase is related to the incorporation of oxygen species into the interstitial sites of the hcp alloy, and the incorporation to form the hcp Zr-O solid solution must be saturated at about the pre-anodizing voltage of 50 V for the present Zr-Ti alloy films of ~490 nm thickness. From the amount of oxide ions in the anodic oxide film formed to 50 V, determined by RBS analysis, the average oxygen concentration in the Zr-Ti alloy film was ~13 at%. Since the Zr_3O phase was formed for the specimens pre-anodized to 80 V and 150 V, further studies were performed for the specimen with pre-anodized to 50 V.

The influence of the oxygen incorporation on the thermal oxidation of the anodized specimen was examined. Figure 6 shows the transmission electron micrographs of a cross-section of the oxygen-incorporated alloy specimen re-anodized at 50 V and then heat-treated at 473 K in air for 72 h. The thickness of the anodic film is only 135 ±3 nm even after heat treatment at 473 K. From the comparison with Fig. 1b, it is obvious that thermal oxidation of the anodized specimens is highly suppressed by the oxygen incorporation. The anodic oxide film is again crystalline, as shown in high resolution observation (Fig. 6b), but an electron diffraction pattern shown in the inset of Fig. 6b indicates the presence of only t-ZrO_2 phase; the m-ZrO_2 phase found in the anodic oxide film formed on the oxygen-free as-deposited alloy is absent. The preferential formation of the t-ZrO_2 phase contributes to the improved dielectric properties as discussed later.

The dielectric properties of the anodic films before and after heat treatments were examined by EIS measurements. Figure 7 shows the change in the Bode plots of the anodized specimens with heat treatment time. The oxygen-free anodized specimen (Fig. 7a) shows a marked decrease in the

impedance within 4 h of heat treatment. The phase shift is close to -90° below 300 Hz before heat treatment, but the value increases after heat treatment. Thus, the dielectric loss is increased after heat treatment. In contrast, the phase shift of the oxygen-incorporated alloy specimens (Fig. 7b) remains almost unchanged below 100 Hz even after heat treatment for 72 h. The impedance at each frequency decreases gradually with heat treatment time, but the change is less significant in comparison with the oxygen-free alloy specimen. EIS measurements were also carried out for anodized Ta specimen. The thermal stability of the anodized Ta is high as shown in Fig. 7c; no changes in impedance and phase shift were found during heat treatment at 473 K. Using an equivalent electric circuit shown in Fig. 7d, the capacitance of the anodic films were determined.

Figure 8a shows the change in the capacitance of the anodic oxide films with heat treatment time at 473 K. The capacitances of the anodic oxide films formed on the three specimens (the oxygen-free and oxygen-incorporated Zr-Ti alloys and Ta) are similar before heat treatment, being 2.5 – 3.0 mF m^{-2}. The capacitance of the oxygen-free alloy specimen increases by nearly one order of magnitude by heat treatment. The increased capacitance is usually beneficial for capacitor application, but the specimen also shows an increase in dissipation factor (tan δ) at 10 Hz with heat treatment (Fig. 8b). Thus, the as-deposited oxygen-free alloy specimen is not suitable for capacitor application. The increase in the capacitance is not consistent with the thickening of the oxide film by heat treatment. The capacitance of an anodic oxide film, C_f, is inversely proportional to the thickness, d, as follows:

$$C_f = \frac{\varepsilon_0 \varepsilon_{ox} S}{d} \quad (2),$$

where ε_0 is the permittivity of vacuum, ε_{ox} is the specific permittivity of anodic oxide, S is the surface area and d is the film thickness. In accord with this equation, the capacitance must decrease as a consequence of film thickening. Nevertheless, the capacitance is highly enhanced after heat treatment. The increase in the capacitance and tan δ due to heat treatment may be associated with the introduction of physical defects in the anodic oxide film during heat treatment. Figure 9 shows scanning electron micrographs of surfaces of the anodic oxide films before and after heat treatment for

72 h. The surface of the anodic film formed on the oxygen-free, as-deposited alloy is relatively flat and smooth (Fig. 9a). No obvious physical defects were found. In contrast, crack-like features were found on the surface after heat treatment (Fig. 9b). EIS measurements were conducted in ammonium pentaborate electrolyte. The electrolyte might penetrate into such cracks, and as a consequence, the capacitance and tan δ increased after heat treatment. Figure 9c shows the surface of the anodic oxide film on the oxygen-incorporated alloy. Healed crack-like features are observed. The cracks in this specimen were developed during heat treatment of the pre-anodized alloy film at 823 K in vacuum, probably associated with the oxygen diffusion from the pre-formed anodic oxide film to the underlying alloy substrate. The volume expansion of the alloy substrate by oxygen incorporation and the simultaneous volume reduction of the anodic oxide film by oxygen removal caused the crack generation. However, re-anodizing of the oxygen-incorporated alloy specimen healed the cracks, as seen in Fig.9c. Even after heat treatment at 473 K in air, the surface morphology remained almost unchanged for the oxygen-incorporated alloy specimen. As a consequence, the increase in the capacitance during the heat treatment was highly suppressed in comparison with the oxygen-free alloy specimen (Fig. 8a). However, the capacitance value became nearly twice that on Ta after heat treatment, while the tan δ value was as low as that on Ta. The increased capacitance of the anodic oxide film on the oxygen-incorporated Zr-Ti alloy after heat treatment in comparison with that on the as-deposited, oxygen-free alloy may be related to the preferential formation of t-ZrO_2 phase, which has much higher permittivity in comparison with m-ZrO_2 [36].

The anodic oxide films formed on Ta used for capacitor application are generally amorphous. The anodized tantalum is rather thermally stable as seen from the constant capacitance of the anodic films during heat treatment at 473 K (Fig. 8). The interference color of the anodized Ta specimen remained unchanged during the heat treatment, indicating negligible change in the thickness of the anodic film. The permittivity of the anodic film formed on Ta was ~28, being consistent with the previous report [5].

Zr forms a crystalline anodic oxide film, in contrast to the formation of amorphous anodic

oxides on many metals, including Ta, Al, Nb and W [39]. The main crystalline phase in the anodic oxide films on Zr is m-ZrO_2. The permittivity of the anodic oxide film on Zr at 100 V in ammonium pentaborate electrolyte was reported to be 23, being smaller than that on Ta [33]. In addition, Zr forms thicker anodic oxide films in comparison with Ta, resulting in the lower capacitance of the anodic oxide films on Zr. Thus, the Zr has not been considered as an electrolytic capacitor material.

However, it was reported that alloying of Zr is effective in enhancing the capacitance of the anodic oxides. The permittivity of anodic oxide films was enhanced to 36 by adding 20 at% Ti to Zr [33]. The enhancement is mainly associated with the phase transformation from mZrO_2 to t-ZrO_2. Further, when Al or Si was added to Zr, anodic oxide films of reduced thickness were formed in addition to the preferential formation of t-ZrO_2, both contributing to the enhancing the capacitance [36,37,40, 41]. The anodic oxide films formed on Zr-Al and Zr-Si alloys consisted of a mixture of t-ZrO_2 nanocrystalline phase and an amorphous matrix enriched in Al or Si species. The latter amorphous phase contributed mainly to the reduction of film thickness.

In the present study, the highly enhanced capacitance of the anodic oxide film on the oxygen-containing Zr-Ti alloy, which is nearly twice that on Ta, is mainly associated with the remarkable increase in the permittivity. The permittivity of the anodic oxide film on the oxygen-containing Zr-Ti alloy after heat treatment for 72 h was as high as 85, which is comparable to that of anatase [42]. The permittivity of t-ZrO_2 was reported to be 34-39 [43]. The high permittivity obtained in this study may be related to the doping of Ti^{4+} in t-ZrO_2, although this is the subject of further study.

For capacitor application of Ta and Nb, a main effort has been directed to reduce the oxygen impurity in Ta and Nb, since the oxygen impurity often induce the crystallization of amorphous anodic oxides [44,45]. For Ta and niobium, crystallization is detrimental because of the increase in the leakage current and enhanced bias dependence of the capacitance [46-48]. In contrast, the findings in the present study demonstrate that the oxygen incorporation must be promoted for capacitor application of the Zr-Ti alloy. The thermal stability of the anodized ally specimen is highly improved

by the oxygen incorporation and, furthermore, the capacitance of the anodic oxide film becomes nearly twice as high as that on Ta. Thus, the oxygen incorporated Zr-Ti alloy is promising as a novel capacitor material.

4. Conclusions

The present study demonstrates the highly improved thermal stability of the anodized Zr-24 at% Ti alloy in air at 473 K by oxygen incorporation. The oxygen-free alloy forms a 125-nm thick anodic oxide film, which contains both m-ZrO_2 and t-ZrO_2 phases, at 50 V in ammonium pentaborate electrolyte. Heat treatment in air at 473 K for 72 h thickens the oxide film to 224 nm and introduces physical defects, causing large degradation of the dielectric properties. However, the oxygen incorporation into the alloy by pre-anodizing and subsequent heat treatment at 823 K in vacuum could avoid the thermal degradation and the capacitance is further increased without increasing the dielectric loss. The increased capacitance is associated with the preferential formation of t-ZrO_2, which has higher permittivity in comparison with m-ZrO_2. The oxygen-incorporated Zr-Ti alloy is a promising material as an alternative of Ta, which natural resource is limited, for electrolytic capacitor application.

Acknowledgments

The present study was supported in part by Nanotechnology Platform" Program of the Ministry of Education, Culture, Sports, Science and Technology (MEXT), Japan.

References

1. Gray JE, Luan B (2002) Protective coatings on magnesium and its alloys — a critical review. J Alloys Compd 336:88-113
2. Thompson GE, Skeldon P, Zhou X, Shimizu K, Habazaki H, Smith CFE (2003) Improving the performance of aerospace alloys. Aircr Eng Aerosp Tec 75 (4):372-379
3. Blawert C, Dietzel W, Ghali E, Song GL (2006) Anodizing treatments for magnesium alloys and

their effecton corrosion resistance in various environments. Adv Eng Mater 8 (6):511-533

4. Watanabe K, Sakairi M, Takahashi H, Hirai S, Yamaguchi S (1999) Formation of Al-Zr composite oxide films on aluminum by sol-gel coating and anodizing. J Electroanal Chem 473 (1-2):250-255

5. Lu Q, Mato S, Skeldon P, Thompson GE, Masheder D, Habazaki H, Shimizu K (2002) Anodic film growth on tantalum in dilute phosphoric acid solution at 20 and 85°C. Electrochim Acta 47 (17):2761-2767

6. Pozdeev-Freeman Y, Gladkikh A (2001) Effect of thermal oxide on the crystallization of the anodic Ta_2O_5 film. J Electron Mater 30 (8):931-936

7. Freeman Y, Alapatt GF, Harrell WR, Lessner P (2012) Electrical characterization of high voltage polymer tantalum capacitors. J Electrochem Soc 159 (10):A1646-A1651

8. Freeman Y, Alapatt GF, Harrell WR, Luzinov I, Lessner P, Qazi J (2013) Anomalous currents in low voltage polymer tantalum capacitors. ECS J Solid State Sci Technol 2 (11):N197-N204

9. Roy P, Berger S, Schmuki P (2011) TiO_2 nanotubes: Synthesis and applications. Angew Chem, Int Ed 50 (13):2904-2939

10. Kowalski D, Kim D, Schmuki P (2013) TiO_2 nanotubes, nanochannels and mesosponge: Self-organized formation and applications. Nano Today 8 (3):235-264

11. Lee W, Park SJ (2014) Porous anodic aluminum oxide: anodization and templated synthesis of functional nanostructures. Chem Rev 114 (15):7487-7556

12. Habazaki H, Ogasawara T, Fushimi K, Shimizu K, Nagata S, Izumi T, Skeldon P, Thompson GE (2008) Inhibition of field crystallization of anodic niobium oxide by incorporation of silicon species. Electrochim Acta 53 (28):8203-8210

13. Habazaki H, Ogasawara T, Konno H, Shimizu K, Nagata S, Skeldon P, Thompson GE (2007) Field crystallization of anodic niobia. Corros Sci 49 (2):580-593

14. Habazaki H, Ogasawara T, Konno H, Shimizu K, Nagata S, Asami K, Takayama K, Skeldon P, Thompson GE (2006) Suppression of field crystallization of anodic niobia by oxygen. J Electrochem Soc 153 (5):B173-B177

15. Habazaki H, Ogasawara T, Konno H, Shimizu K, Asami K, Nagata S, Takayama K, Skeldon P, Thompson G Field crystallization of anodic niobia on Nb-O substrates In: Fujimoto S, Akiyama E, Habazaki H, Macdougall B (eds) ECS Trans, Los Angeles, 2006. vol 4. The Electrochemical Society, pp 343-349

16. Nagahara K, Sakairi M, Takahashi H, Nagata S, Matsumoto K, Takayama K, Oda Y (2004) Influence of current density on the structure and dielectric properties of anodic oxide films on niobium. J Surf Finish Soc Jpn 55 (12):943-951

17. Nagahara K, Sakairi M, Takahashi H, Matsumoto K, Takayama K, Oda Y (2004) Change in the structure and dielectric properties of niobium anodic oxide films during potentiostatic anodizing. Elechemistry 72 (9):624-632

18. Lakhiani DM, Shreir LL (1960) Crystallization of amorphous Nb oxide during anodic oxidation. Nature 188:49-50

19. Modestov AD, Davydov AD (1999) Capacitance and photocurrent study of electronic properties of anodic oxide films on Nb and Ta. Evaluation of the ionized donor concentration profile in Nb_2O_5 film. J Electroanal Chem 460:214-225

20. Habazaki H, Ogasawara T, Konno H, Shimizu K, Asami K, Saito K, Nagata S, Skeldon P, Thompson GE (2005) Growth of anodic oxide films on oxygen-containing niobium. Electrochim Acta 50 (27):5334-5339

21. Habazaki H, Matsuo T, Konno H, Shimizu K, Nagata S, Takayama K, Oda Y, Skeldon P, Thompson GE (2003) Formation of N_2O gas bubbles in anodic films on NbN_x alloys. Thin Solid Films 429 (1-2):159-166

22. Habazaki H, Matsuo T, Konno H, Shimizu K, Nagata S, Matsumoto K, Takayama K, Oda Y, Skeldon P, Thompson GE (2003) Influence of silicon species on the electric properties of anodic niobia. Electrochim Acta 48 (23):3519-3526

23. Habazaki H, Matsuo T, Konno H, Shimizu K, Matsumoto K, Takayama K, Oda Y, Skeldon P, Thompson GE (2003) Analysis of anodic films on Nb and NbN_x by glow discharge optical

emission spectroscopy. Surf Interface Anal 35 (7):618-622

24. Aladjem A (1973) Anodic oxidation of titanium and its alloys. J Mater Sci 8:688-704

25. Dyer CK, Leach JSL (1978) Breakdown and efficiency of anodic oxide growth on titanium. J Electrochem Soc 125:1032-1038

26. Habazaki H, Uozumi M, Konno H, Shimizu K, Skeldon P, Thompson GE (2003) Crystallization of anodic titania on titanium and its alloys. Corros Sci 45 (9):2063-2073

27. Habazaki H, Uozumi M, Konno H, Nagata S, Shimizu K (2003) Formation of barrier-type amorphous anodic films on Ti-Mo alloys. Surf Coat Technol 169:151-154

28. Habazaki H, Uozumi M, Konno H, Shimizu K, Nagata S, Asami K, Matsumoto K, Takayama K, Oda Y, Skeldon P, Thompson GE (2003) Influences of structure and composition on growth of anodic oxide films on Ti-Zr alloys. Electrochim Acta 48 (20-22):3257-3266

29. Habazaki H, Uozumi M, Konno H, Shimizu K, Nagata S, Takayama K, Oda Y, Skeldon P, Thompson GE (2005) Influence of film composition on the structure and dielectric properties of anodic films on Ti-W alloys. J Electrochem Soc 152 (8):B263-B270

30. Tanvir MT, Fushimi K, Shimizu K, Nagata S, Skeldon P, Thompson GE, Habazaki H (2007) Influence of silicon on the growth of barrier-type anodic films on titanium. Electrochim Acta 52 (24):6834-6840

31. Di Franco F, Santamaria M, Di Quarto F, Macaluso R, Mosca M, Cali C (2014) Electrochemical fabrication and physicochemical characterization of metal/high-k insulating oxide/polymer/electrolyte junctions. J Phys Chem C 118 (51):29973-29980

32. Di Franco F, Bocchetta P, Cali C, Mosca M, Santamaria M, Di Quarto F (2011) Electrochemical fabrication of metal/oxide/conducting polymer junction. J Electrochem Soc 158 (1):H50-H54

33. Habazaki H, Shimizu K, Nagata S, Asami K, Takayama K, Oda Y, Skeldon P, Thompson GE (2005) Inter-relationship between structure and dielectric properties of crystalline anodic zirconia. Thin Solid Films 479 (1-2):144-151

34. Santamaria M, Di Quarto F, Habazaki H (2008) Influences of structure and composition on the

photoelectrochemical behaviour of anodic films on Zr and Zr-20 at.% Ti. Electrochim Acta 53 (5):2272-2280

35. Climent-Font A, Watjen V, Bax H (1992) Quantitative RBS analysis using RUMP. On the accuracy of the He stopping in Si. Nucle Instr and Meth B71:81-86

36. Habazaki H, Koyama S, Aoki Y, Sakaguchi N, Nagata S (2011) Enhanced capacitance of composite anodic ZrO_2 films comprising high permittivity oxide nanocrystals and highly resistive amorphous oxide matrix. ACS App Mater Interfaces 3 (7):2665-2670

37. Koyama S, Aoki Y, Sakaguchi N, Nagata S, Habazaki H (2010) Phase transformation and capacitance enhancement of anodic ZrO_2-SiO_2. J Electrochem Soc 157 (12):C444-C451

38. Brossmann U, Wurschum R, Sodervall U, Schaefer HE (1999) Oxygen diffusion in ultrafine grained monoclinic ZrO_2. J Appl Phys 85 (11):7646-7654

39. Pringle JPS (1980) The anodic oxidation of superimposed metallic layers: theory. Electrochim Acta 25:1423-1437

40. Koyama S, Y.Aoki, Nagata S, Habazaki H (2011) Formation and dielectric properties of anodic oxide films on Zr-Al alloys. J Solid State Electrochem 15:2221-2229

41. Koyama S, Aoki Y, Nagata S, Kimura H, Habazaki H (2010) Amorphous-to-crystalline transition of silicon-incorporated anodic ZrO_2 and improved dielectric properties. Electrochim Acta 55 (9):3144-3151

42. San Andres E, Toledano-Luque M, del Prado A, Navacerrada MA, Martil I, Gonzalez-Diaz G, Bohne W, Rohrich J, Strub E (2005) Physical properties of high pressure reactively sputtered TiO_2. J Vacuum Sci Technol A 23 (6):1523-1530

43. Thompson DP, Dickins AM, Thorp JS (1992) The Dielectric-properties of zirconia. J Mater Sci 27 (8):2267-2271

44. Pozdeev-Freeman Y, Gladkikh A, Karpovski M, Palevski A (1998) Effect of dissolved oxygen on thermal oxidation in Ta2O5/Ta sandwiches. J Electronic Mater 27:1034-1037

45. Pozdeev-Freeman Y, Rozenberg Y, Gladkikh A, Karpovski M, Palevski A (1998) Critical oxygen

content in porous anodes of solid tantalum capacitors. J Mater Sci: Mater Electron 9 (4):309-311

46. Vermilyea DA (1955) The crystallization of anodic tantalum oxide films in the presence of a strong electric field. J Electrochem Soc 102:207-214

47. Nagahara K, Sakairi M, Takahashi H, Matsumoto K, Takayama K, Oda Y (2007) Mechanism of formation and growth of sunflower-shaped imperfections in anodic oxide films on niobium. Electrochim Acta 52 (5):2134-2145

48. Su X, Viste M, Hossick-Schott J, Yang L, Sheldon BW (2015) Reassessment of degradation mechanisms in anodic tantalum oxide capacitors under high electric fields. J Mater Sci 50 (2):960-969.

Figure captions

Fig. 1 Transmission electron micrographs of cross-sections of the magnetron-sputtered Zr-24 at% Ti alloy anodized at 50 V for 30 min in 0.01 mol dm^{-3} ammonium pentaborate electrolyte at 293 K (a) before and (b) after heat treatment in air at 473 K for 72 h. (c) high magnification micrograph of the anodic oxide film in (a).

Fig. 2 (color online) GDOES elemental depth profiles of the magnetron-sputtered Zr-24 at% Ti alloy anodized at 50 V for 30 min in 0.01 mol dm^{-3} ammonium pentaborate electrolyte at 293 K (a) before and (b) after heat treatment in air at 473 K for 72 h.

Fig. 3 (color online) Experimental and simulated RBS spectra of the magnetron-sputtered Zr-24 at% Ti alloy anodized at 50 V for 30 min in 0.01 mol dm^{-3} ammonium pentaborate electrolyte at 293 K (a) before and (b) after heat treatment in air at 473 K for 72 h.

Fig. 4 GI-XRD patterns of the magnetron-sputtered Zr-24 at% Ti alloy anodized at 50 V for 30 min in 0.01 mol dm^{-3} ammonium pentaborate electrolyte at 293 K before and after heat treatment in air at 473 K for 72 h.

Fig. 5 (a) GI-XRD patterns of the magnetron-sputtered Zr-24 at% Ti alloy pre-anodized to several voltages at 50 A m^{-2} in 0.01 mol dm^{-3} ammonium pentaborate electrolyte at 293 K and subsequent vacuum heat treatment at 823 K for 1 h and (b) the change in (103) lattice spacing of the hcp alloy phase in (a) with pre-anodizing voltage.

Fig. 6 (a) Transmission electron micrograph of a cross-section of the magnetron-sputtered Zr-24 at% Ti alloy anodized at 50 V for 30 min in 0.01 mol dm^{-3} ammonium pentaborate electrolyte at 293 K. Prior to anodizing, the alloy was pre-anodized to 50 V at 50 A m^{-2} in the same electrolyte and then

vacuum heat-treated at 823 K for 1 h for oxygen incorporation. (b) high magnification micrograph of the anodic oxide film in (a).

Fig. 7 (color online) EIS Bode plots of the magnetron-sputtered, (a) oxygen-free and (b) oxygen-incorporated Zr-24 at% Ti alloy and (c) Ta anodized at 50 V for 30 min in 0.01 mol dm^{-3} ammonium pentaborate electrolyte at 293 K before and after heat treatment in air at 473 K for various periods of time.

Fig. 8 (color online) Change in (a) capacitance and (b) tan δ with heat treatment time for the anodic oxide films formed on the magnetron-sputtered, oxygen-free and oxygen-incorporated Zr-Ti alloy and Ta at 50 V for 30 min in 0.01 mol dm^{-3} ammonium pentaborate electrolyte at 293 K. Heat treatment was performed in air at 473 K.

Fig. 9 Scanning electron micrographs of surfaces of the magnetron-sputtered, (a,b) oxygen-free and (c,d) oxygen-incorporated Zr-Ti alloy anodized at 50 V for 30 min in 0.01 mol dm^{-3} ammonium pentaborate electrolyte at 293 K (a,c) before and (b,d) after teat treatment in air at 473 K.

Table 1 Results of RBS analysis of the Zr-24 at% Ti alloy specimens anodized to 50 V at a constant current density of 50 A m^{-2} in 0.01 mol dm^{-3} ammonium pentaborate electrolyte before and after heat treatment at 473 K in air for 72 h.

	Oxide thickness (nm)	Oxide composition	Density (g cm^{-3})
Before heat treatment	125	$(Zr_{0.76}Ti_{0.24})O_2$	4.14
After heat treatment	224	$(Zr_{0.76}Ti_{0.24})O_2$	4.50

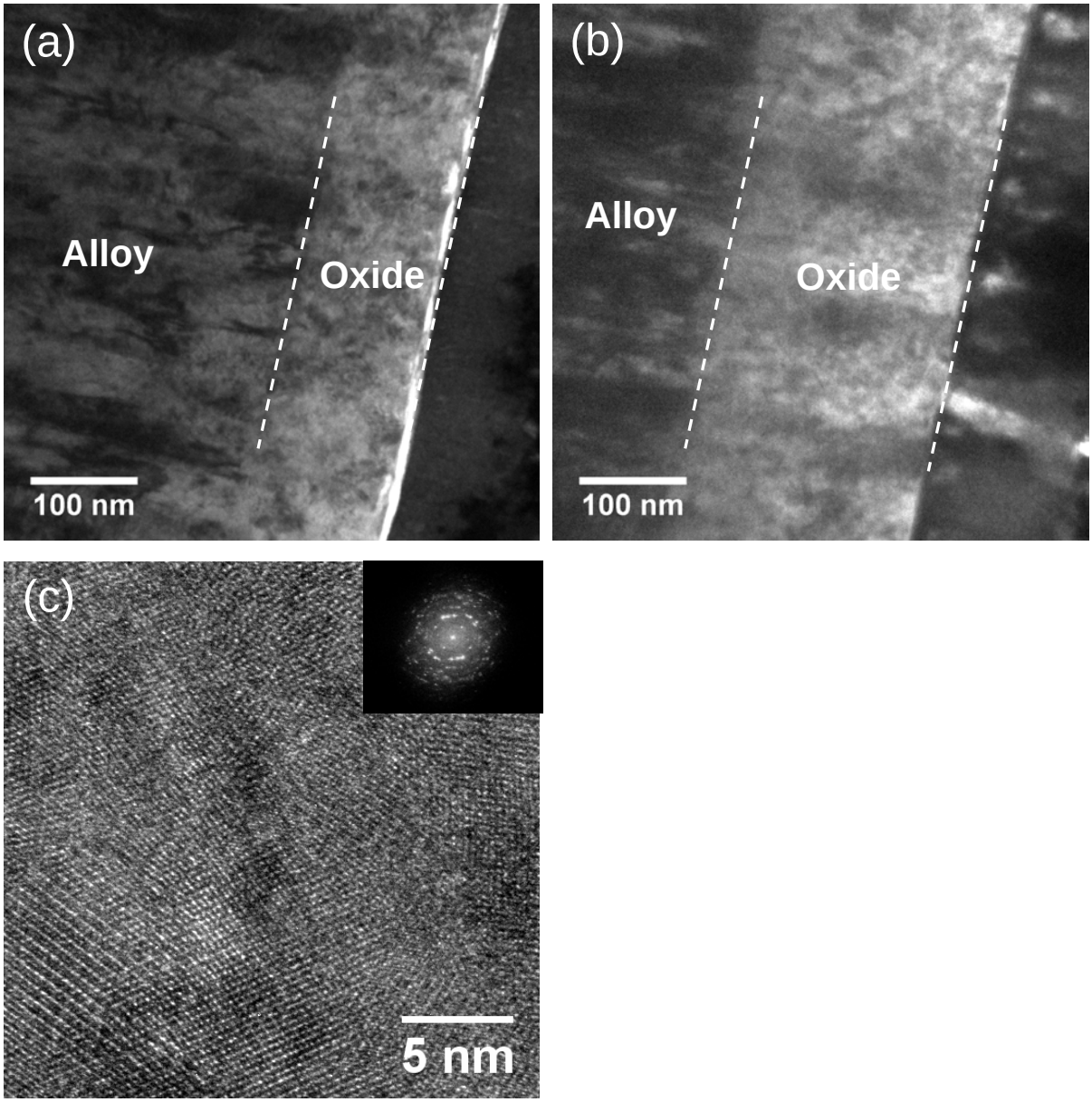

Fig. 1 Transmission electron micrographs of cross-sections of the magnetron-sputtered Zr-24 at% Ti alloy anodized at 50 V for 30 min in 0.01 mol dm^{-3} ammonium pentaborate electrolyte at 293 K (a) before and (b) after heat treatment in air at 473 K for 72 h. (c) high magnification micrograph of the anodic oxide film in (a).

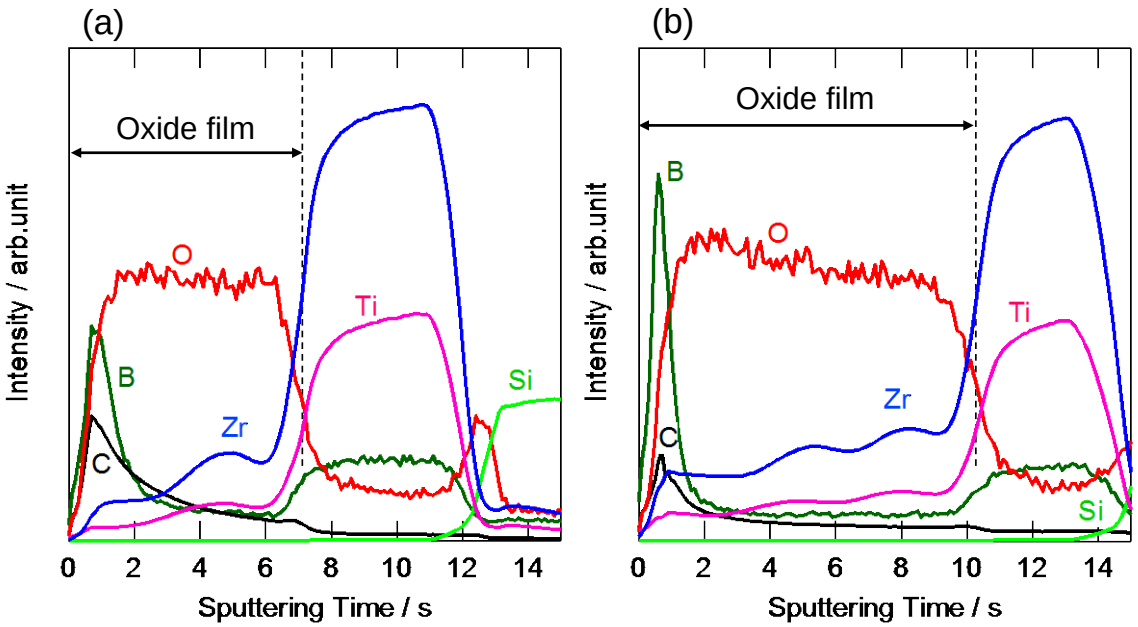

Fig. 2 (color online) GDOES elemental depth profiles of the magnetron-sputtered Zr-24 at% Ti alloy anodized at 50 V for 30 min in 0.01 mol dm^{-3} ammonium pentaborate electrolyte at 293 K (a) before and (b) after heat treatment in air at 473 K for 72 h.

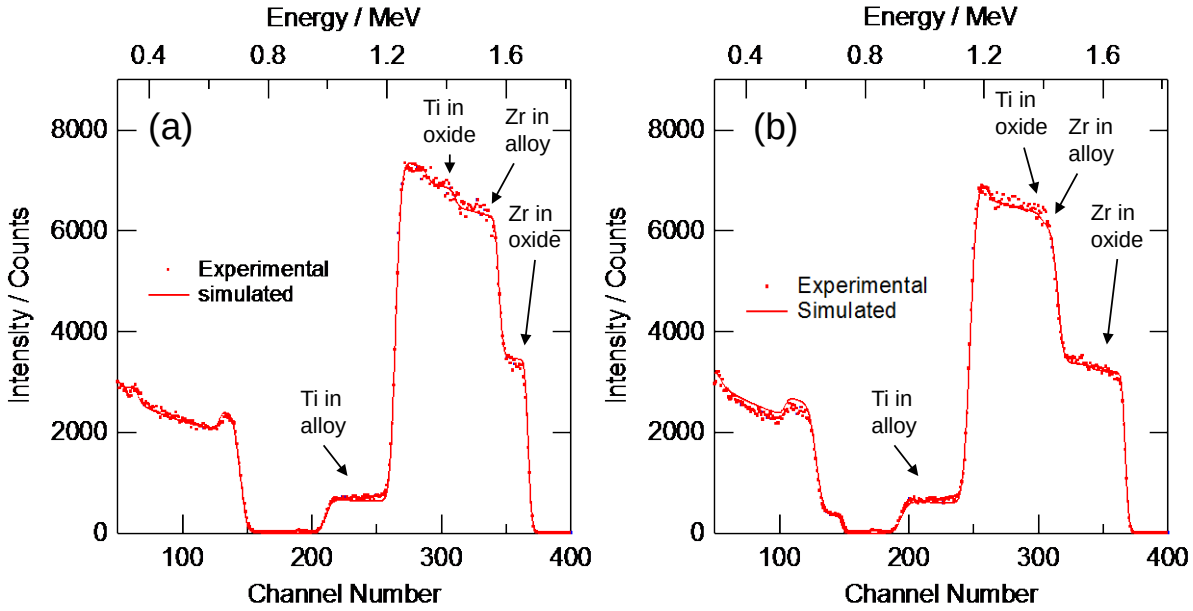

Fig. 3 (color online) Experimental and simulated RBS spectra of the magnetron-sputtered Zr-24 at% Ti alloy anodized at 50 V for 30 min in 0.01 mol dm^{-3} ammonium pentaborate electrolyte at 293 K (a) before and (b) after heat treatment in air at 473 K for 72 h.

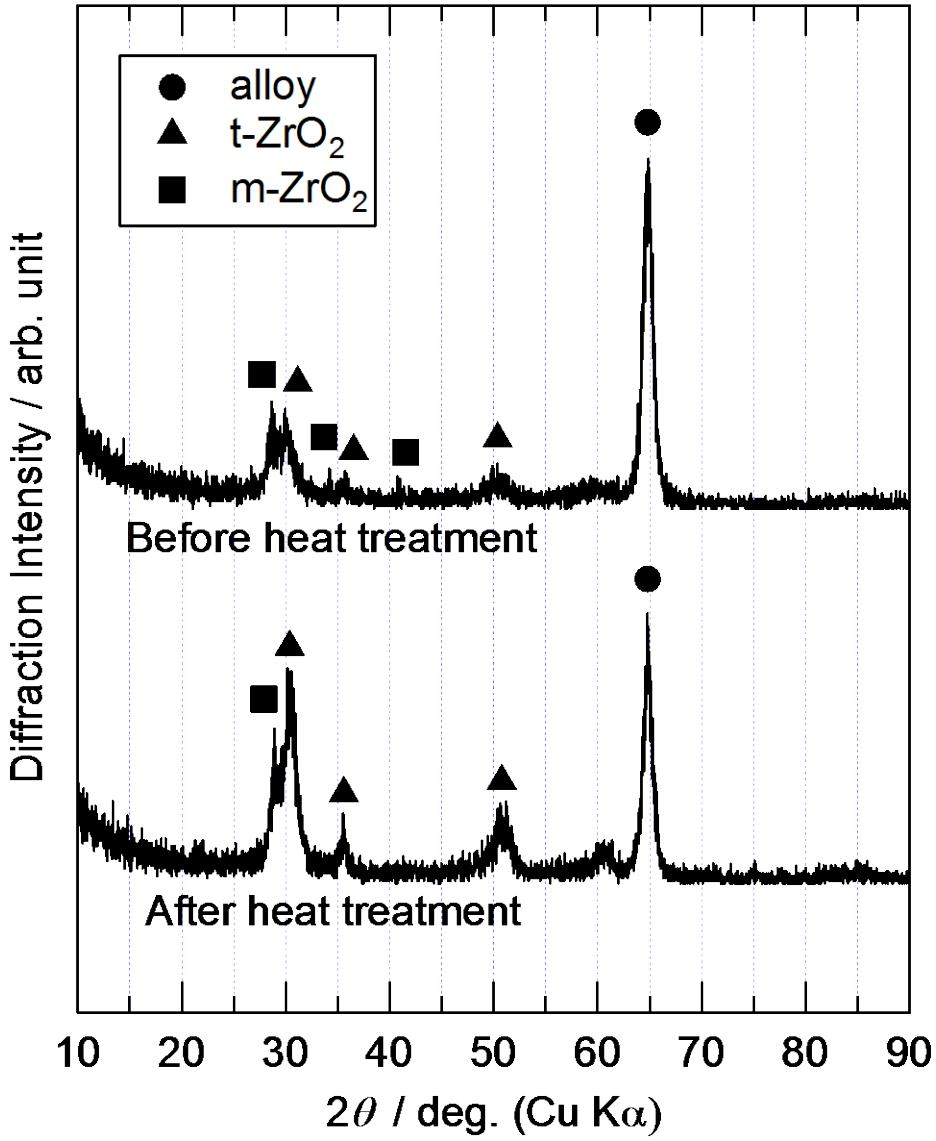

Fig. 4 GI-XRD patterns of the magnetron-sputtered Zr-24 at% Ti alloy anodized at 50 V for 30 min in 0.01 mol dm^{-3} ammonium pentaborate electrolyte at 293 K before and after heat treatment in air at 473 K for 72 h.

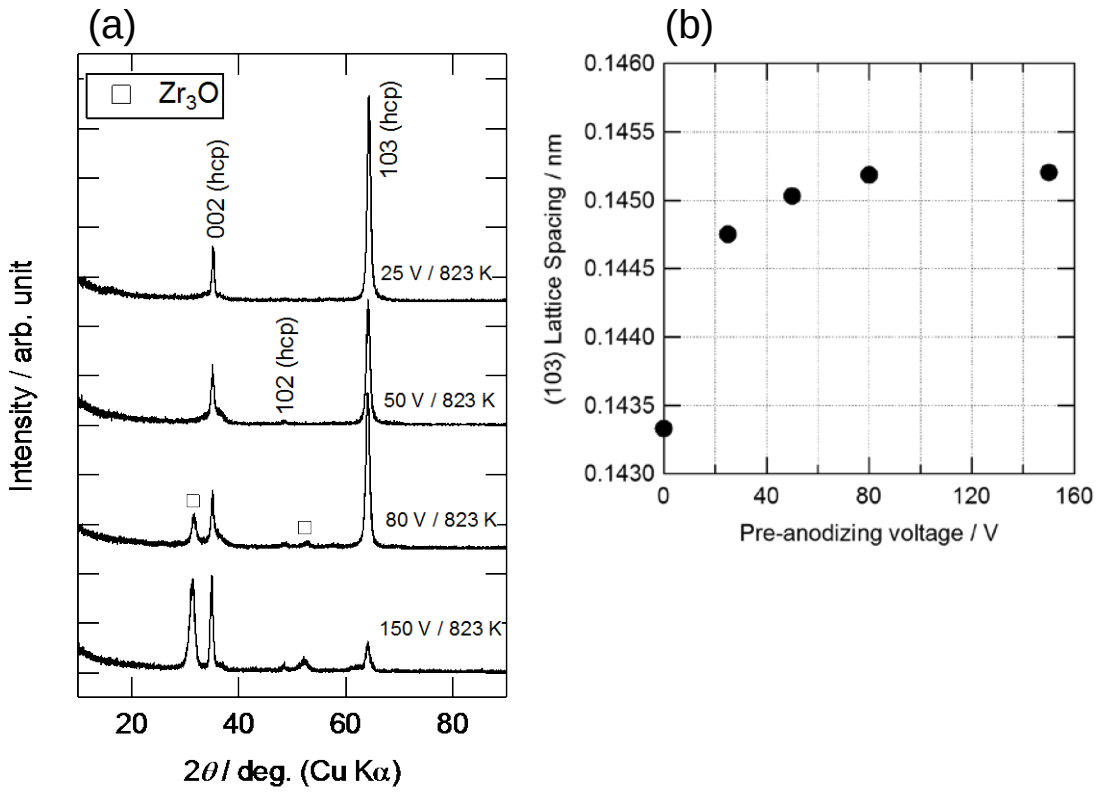

Fig. 5 (a) GI-XRD patterns of the magnetron-sputtered Zr-24 at% Ti alloy pre-anodized to several voltages at 50 A m^{-2} in 0.01 mol dm^{-3} ammonium pentaborate electrolyte at 293 K and subsequent vacuum heat treatment at 823 K for 1 h and (b) the change in (103) lattice spacing of the hcp alloy phase in (a) with pre-anodizing voltage.

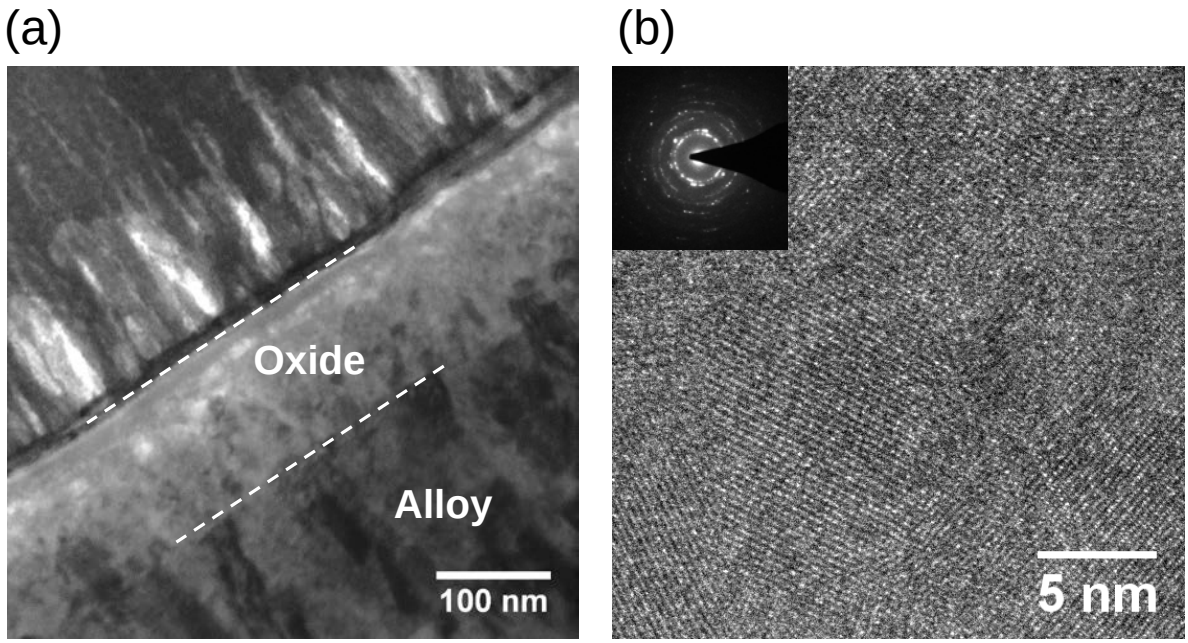

Fig. 6 (a) Transmission electron micrograph of a cross-section of the magnetron-sputtered Zr-24 at% Ti alloy anodized at 50 V for 30 min in 0.01 mol dm^{-3} ammonium pentaborate electrolyte at 293 K. Prior to anodizing, the alloy was pre-anodized to 50 V at 50 A m^{-2} in the same electrolyte and then vacuum heat-treated at 823 K for 1 h for oxygen incorporation. (b) high magnification micrograph of the anodic oxide film in (a).

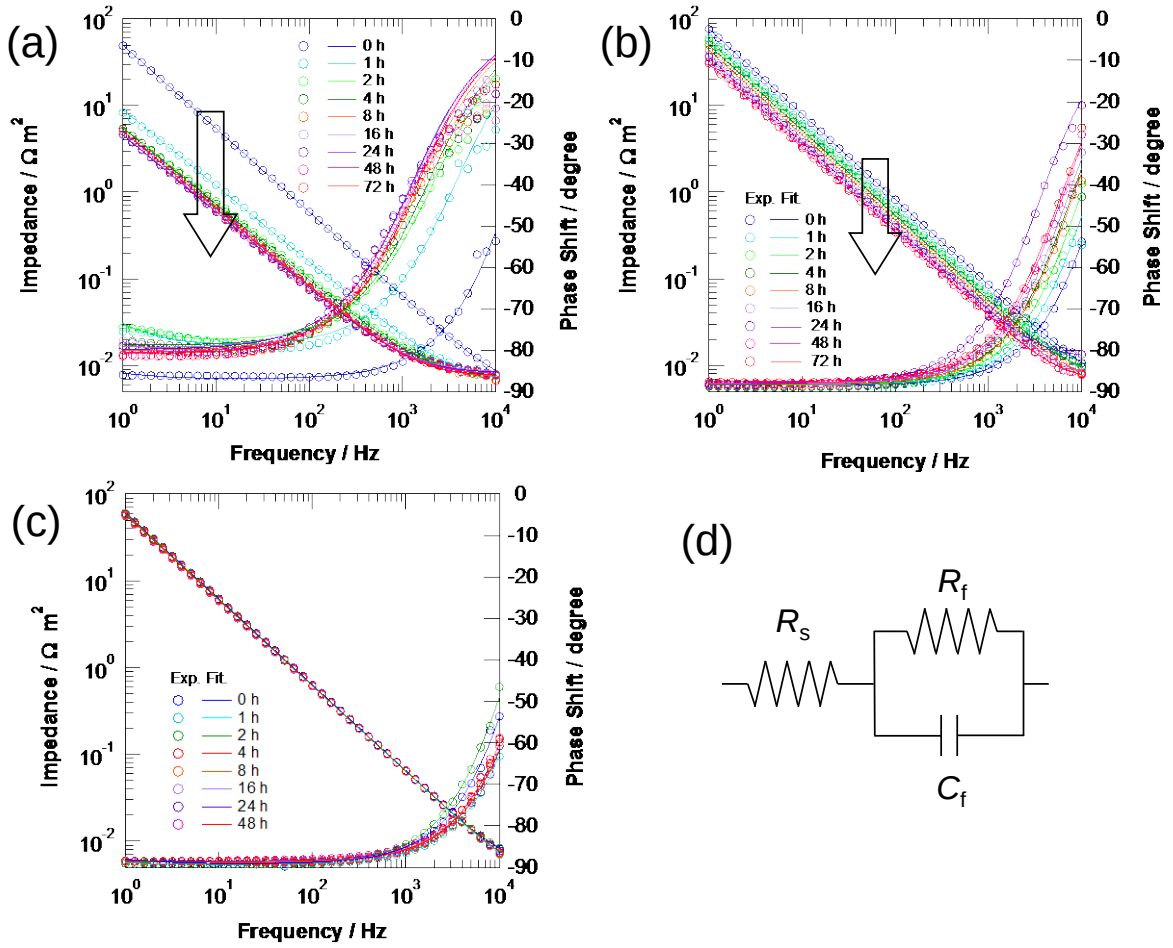

Fig. 7 (color online) EIS Bode plots of the magnetron-sputtered, (a) oxygen-free and (b) oxygen-incorporated Zr-24 at% Ti alloy and (c) Ta anodized at 50 V for 30 min in 0.01 mol dm^{-3} ammonium pentaborate electrolyte at 293 K before and after heat treatment in air at 473 K for various periods of time.

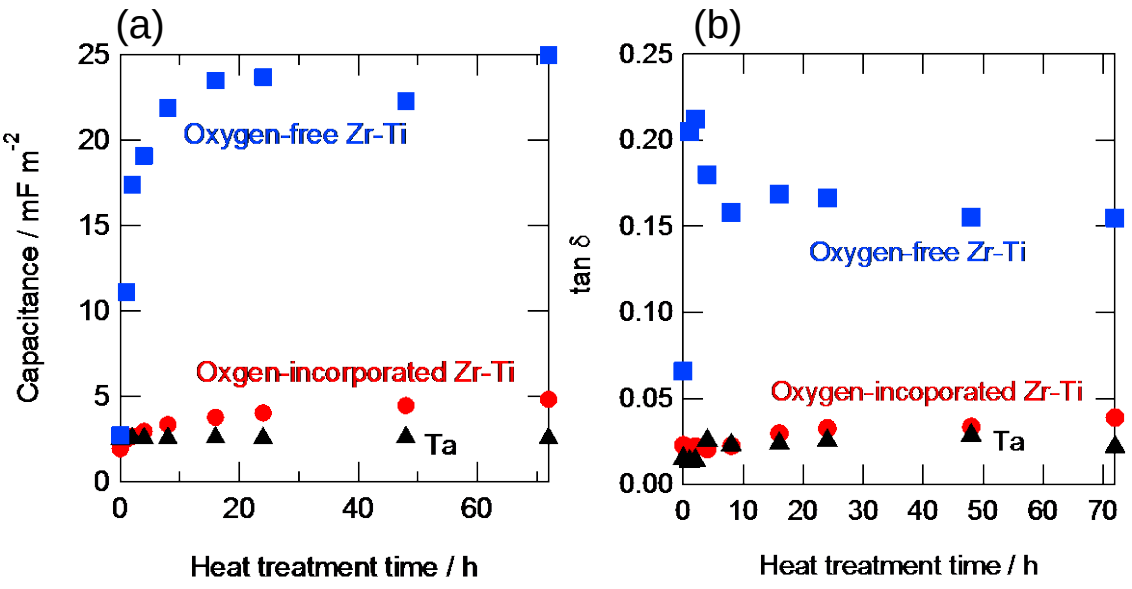

Fig. 8 (color online) Change in (a) capacitance and (b) tan δ with heat treatment time for the anodic oxide films formed on the magnetron-sputtered, oxygen-free and oxygen-incorporated Zr-Ti alloy and Ta at 50 V for 30 min in 0.01 mol dm^{-3} ammonium pentaborate electrolyte at 293 K. Heat treatment was performed in air at 473 K.

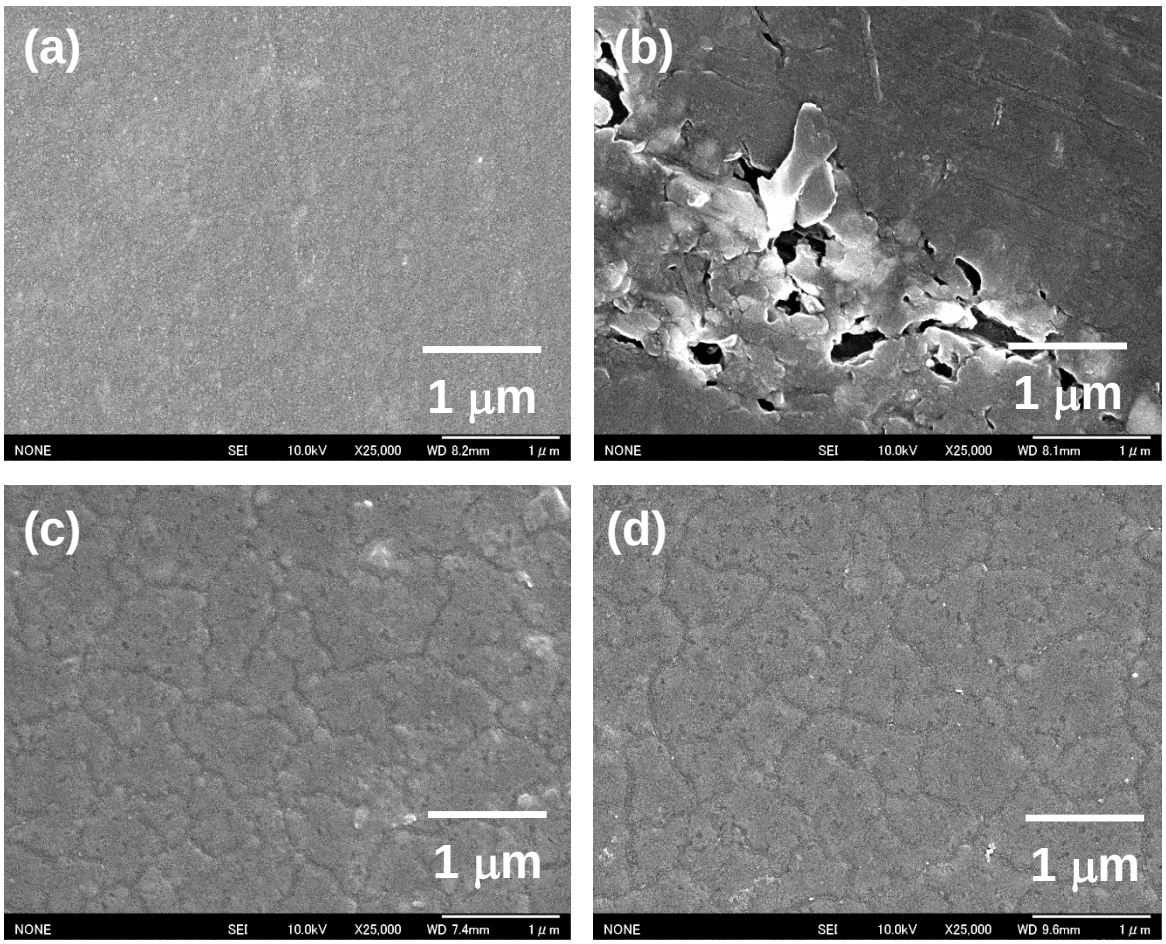

Fig. 9 Scanning electron micrographs of surfaces of the magnetron-sputtered, (a,b) oxygen-free and (c,d) oxygen-incorporated Zr-Ti alloy anodized at 50 V for 30 min in 0.01 mol dm^{-3} ammonium pentaborate electrolyte at 293 K (a,c) before and (b,d) after teat treatment in air at 473 K.